Charge density wave behavior and order-disorder in the antiferromagnetic metallic series $Eu(Ga_{1-x}Al_x)_4$

Macy Stavinoha,[1,*] Joya A. Cooley,[2] Stefan G. Minasian,[3] Tyrel M. McQueen,[4,5,6] Susan M. Kauzlarich,[2] C.-L. Huang,[7] and E. Morosan[1,7]

[1]*Department of Chemistry, Rice University, Houston, Texas 77005, USA*
[2]*Department of Chemistry, University of California, Davis, California 95616, USA*
[3]*Chemical Sciences Division, Lawrence Berkeley National Laboratory, Berkeley, California 94720, USA*
[4]*Institute for Quantum Matter and Department of Physics and Astronomy, Johns Hopkins University, Baltimore, Maryland 21218, USA*
[5]*Department of Chemistry, Johns Hopkins University, Baltimore, Maryland 21218, USA*
[6]*Department of Materials Science and Engineering, Johns Hopkins University, Baltimore, Maryland 21218, USA*
[7]*Department of Physics and Astronomy, Rice University, Houston, Texas 77005, USA*

(Received 4 April 2018; published 23 May 2018)

The solid solution $Eu(Ga_{1-x}Al_x)_4$ was grown in single crystal form to reveal a rich variety of crystallographic, magnetic, and electronic properties that differ from the isostructural end compounds $EuGa_4$ and $EuAl_4$, despite the similar covalent radii and electronic configurations of Ga and Al. Here we report the onset of magnetic spin reorientation and metamagnetic transitions for $x = 0$–1 evidenced by magnetization and temperature-dependent specific heat measurements. T_N changes nonmonotonously with x, and it reaches a maximum around 20 K for $x = 0.50$, where the a lattice parameter also shows an extreme (minimum) value. Anomalies in the temperature-dependent resistivity consistent with charge density wave behavior exist only for $x = 0.50$ and 1. Density functional theory calculations show increased polarization between the Ga-Al covalent bonds in the $x = 0.50$ structure compared to the end compounds, such that crystallographic order and chemical pressure are proposed as the causes of the charge density wave behavior.

DOI: 10.1103/PhysRevB.97.195146

I. INTRODUCTION

The interplay of structural, magnetic, and electronic properties of rare-earth-based intermetallics often results in emergent phenomena and competing ground states, such as unconventional superconductivity, heavy fermion behavior, intermediate valence, and quantum criticality [1]. Particularly, pressure, magnetic field, or chemical doping in Ce and Yb compounds in their magnetic or nonmagnetic sublattices has been extensively used to tune the balance between their versatile ground states [2–4]. Comparatively less work has been done to explore the effects of pressure or doping in Eu-based intermetallics, even though Eu presents similar opportunities to tune the ground state through valence fluctuations between magnetic Eu^{2+} and nonmagnetic Eu^{3+} ions [5]. In this study, we explore the effects of isovalent doping in the $Eu(Ga_{1-x}Al_x)_4$ series, motivated by the wide range of apparently conflicting results observed when tuning the properties of the end compounds $EuGa_4$ and $EuAl_4$.

Previous studies on single crystals of the stoichiometric compounds $EuGa_4$ and $EuAl_4$ revealed that the two show similar magnetic behavior, with antiferromagnetic (AFM) ordering and very similar Neél temperatures $T_N = 15$ and 15.4 K, respectively [6–8]. The compounds are isostructural, forming in a tetragonal crystal structure consisting of two distinct transition metal sites, forming a covalently bound anionic framework with divalent body-centered cations. The structural and magnetic similarities between these two compounds may be easily understood considering the chemical similarities of Ga and Al: they are isovalent, with very close covalent radii of 1.22 and 1.21 Å, respectively [9]. However, drastic differences have also been noted with either doping or applied pressure, which cannot be readily explained. While no evidence for mass renormalization has been reported in $EuAl_4$, electrical resistivity measurements have suggested heavy fermion behavior in $EuGa_4$ [7,8]. At ambient pressure, a plausible charge density wave (CDW) was reported for $EuAl_4$ below $T^* = 140$ K, and increasing pressure suppressed T^* to zero for $p = 2.5$ GPa. However, in $EuGa_4$, a plausible CDW is observed *only* under applied pressure, with $T^* = 105$ K for $p = 0.75$ GPa, which subsequently increased to 160 K for $p = 2.15$ GPa. Doping EuM_4 (M = Ga or Al) on either the magnetic (Eu) or nonmagnetic (M) sublattice has also shown notable changes in the magnetic, electronic, and crystallographic properties. When Eu is substituted by Yb in $(Eu_{0.5}Yb_{0.5})Ga_4$, T_N is suppressed to 13 K [10]. On the other hand, doping $EuGa_4$ in the nonmagnetic sublattice has shown that the AFM order is suppressed to $T_N = 9.6$ and 6.3 K in polycrystalline $Eu(Ga_{1-x}A_x)_4$, where $(A,x) = (Mg, 0.14)$ or (Li, 0.18), respectively [11]. In contrast, $EuAl_4$ doped with Si resulted in ferromagnetic (FM) order below $T_C = 17$ K in $Eu(Al_{0.75}Si_{0.25})_4$ [12].

The versatile interplay between spin and charge degrees of freedom in EuM_4 motivates the current systematic study of the solid solution between the Ga and Al end compounds in the series $Eu(Ga_{1-x}Al_x)_4$ with $x = 0$ to 1. Such a substitution

*Corresponding author: macylauren@rice.edu

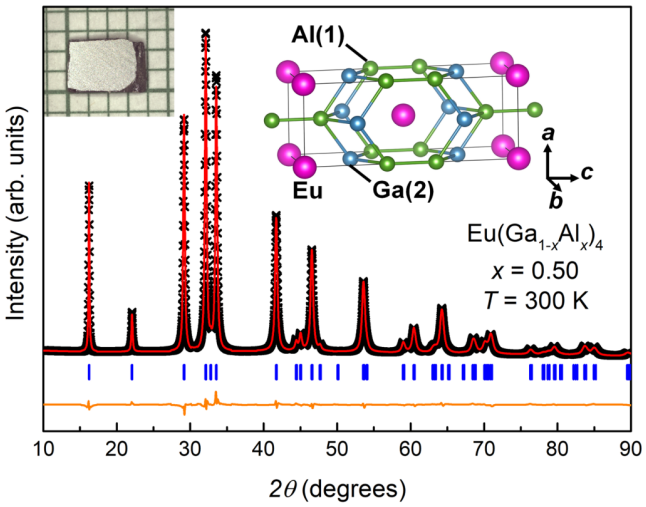

FIG. 1. Powder x-ray diffraction (black symbols) of a doped single crystal of $Eu(Ga_{1-x}Al_x)_4$ with $x = 0.50$ indicates that this crystal (and all crystals in this doped series) crystallizes in the $I4/mmm$ space group with no significant flux inclusion or impurity phases. The red line is the diffraction pattern calculated from Rietveld refinement, and the blue ticks are the calculated peak positions. The orange line is the difference between the measured points and the calculated diffraction. The left inset is a picture of a crystal with each square equal to 1×1 mm^2, and the right inset shows the tetragonal crystal structure.

should minimize the chemical effects brought about by doping since replacing Ga with isoelectronic and similarly sized Al does not change the electron count or the volume of the unit cell (and hence the chemical pressure). Thermodynamic and transport measurements on $Eu(Ga_{1-x}Al_x)_4$ single crystals reveal strong correlations between the structural, magnetic, and electronic properties. The compounds remain tetragonal with space group $I4/mmm$ at room temperature for the whole doping range, with Ga and Al preferentially occupying one or the other of the two transition metal element sites. Remarkably, for $x = 0.50$, the two transition metals fully separate into two sublattices and form an ordered structure $EuGa_2Al_2$ with a minimum unit cell volume in the series. This, in turn, favors the occurrence of a plausible CDW state at ambient pressure at $T^* = 51$ K, while T_N is maximum in this composition at $\sim$20 K. These results should be contrasted with those from isoelectronic doping (Ca^{2+} or Sr^{2+}) or hole doping (La^{3+}) [13] in $EuGa_4$ on the magnetic sublattice, where in some cases structural distortions preclude the occurrence of a CDW transition down to 2 K.

II. EXPERIMENTAL METHODS

Single crystals of $Eu(Ga_{1-x}Al_x)_4$ were grown by a self-flux technique. Elemental metals were assembled in alumina crucibles with a 1:9 ratio of Eu:Ga/Al. In a typical growth, the metals were melted and homogenized at 900 °C and cooled to 700 °C at 3 °C/h in an inert argon atmosphere. Single crystals were separated from the flux using centrifugation through an alumina strainer placed between the crucibles. Powder x-ray diffraction was performed at ambient and low temperatures using a Bruker D8 Advance equipped with a Bruker MTC-LOWTEMP sample stage with Cu $K\alpha$ radiation. Rietveld refinements were done using the FULLPROF program suite [14]. single crystal x-ray diffraction was performed using a Bruker Apex II diffractometer or a Rigaku SCX Mini diffractometer with Mo $K\alpha$ radiation. Integration of raw frame data was done using Bruker Apex II software or CRYSTALCLEAR 2.0. Refinement of the diffraction data was performed using the XPREP and SHELXTL software packages.

Electron microprobe analysis (EMPA) was performed using a Cameca SX-100 electron probe microanalyzer with a wavelength-dispersive spectrometer. An accelerating potential of 15 kV and a beam current of 20 nA in a 1 μm fixed beam were used to collect elemental intensities from 15 representative points on a polished surface of each crystal. The composition of each crystal was determined using the averages and standard deviations of the elemental intensities of Eu, Ga, and Al. The elemental intensities of Eu and Ga were determined from a standard sample of $EuGa_4$, and the elemental intensity of Al was similarly determined from a standard sample of Al_2O_3. Chemical formulas for each crystal were calculated assuming five atoms per formula unit and full occupancy of the Ga/Al site. The compositions obtained from EMPA and free variable refinement of the single crystal x-ray diffraction data were used to determine the doping fractions reported throughout this work with an error of $\pm 3\%$ in the composition.

Single energy images, elemental maps, and Eu $M_{5,4}$-edge x-ray absorption spectra (XAS) were acquired using the scanning transmission x-ray microscope instrument at the spectromicroscopy beamline 10ID-1 at the Canadian Light Source according to data acquisition methodology described previously [15,16]. Samples were prepared by grinding crystals of the analyte into a fine powder with a mortar and pestle and brushing the powder onto carbon support films (3–4 nm carbon, Electron Microscopy Sciences) with a fiber, which arranged a large number of micron-sized particles in a compact area suitable for Eu $M_{5,4}$-edge XAS.

The dc magnetic susceptibility measurements were performed using a Quantum Design magnetic properties measurement system. Specifc heat measurements were performed by adiabatic thermal relaxation technique using a Quantum Design physical properties measurement system (PPMS). Temperature-dependent ac resistivity measurements were performed using a Quantum Design PPMS with current $i = 2$ mA and $f = 462.02$ Hz for a duration of 7 s with $i||ab$.

III. RESULTS

A. Crystallography

Single crystals of $Eu(Ga_{1-x}Al_x)_4$ with dimensions of approximately $3 \times 2 \times 1$ mm^3 were grown for $x = 0$, 0.18, 0.33, 0.50, 0.68, and 1. Powder x-ray diffraction at 300 K indicates that all crystals in this series crystallize in the tetragonal $I4/mmm$ space group. A typical Rietveld analysis is shown for $x = 0.50$ in Fig. 1, indicating no significant flux inclusions or impurity phases. Temperature-dependent powder x-ray diffraction measurements (see the Appendix, Fig. 7) on $EuAl_4$ at $T = 300$ and 93 K confirm that the tetragonal crystal structure is preserved down to low temperatures with no structural phase transition, as was reported in some isostructural

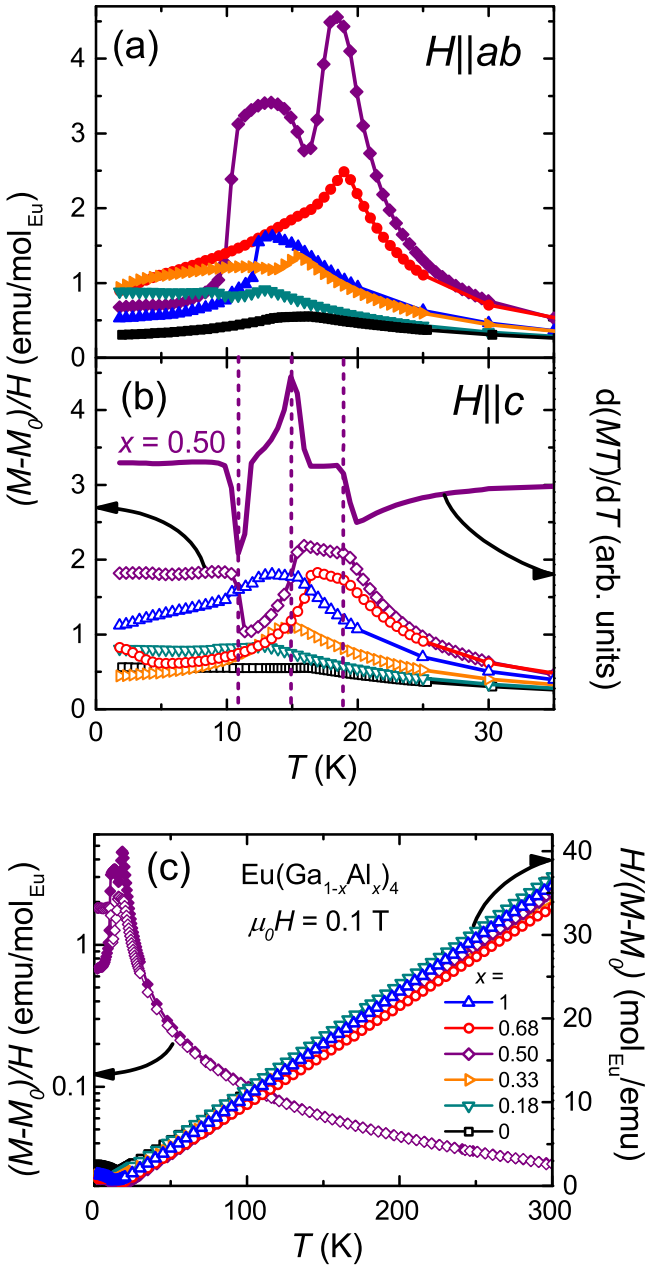

FIG. 2. Temperature-dependent magnetic susceptibility data with (a) $H \| ab$ and (b) $H \| c$ (left axis). Peaks determined from $d(MT)/dT$ were used to indicate T_N and spin reorientation transition temperatures (right axis). (c) At high temperatures, $(M - M_0)/H$ for $x = 0.50$ with solid symbols representing $H \| ab$ and open symbols representing $H \| c$ (left axis). The inverse magnetic susceptibility of the polycrystalline average indicates that these crystals show Curie-Weiss behavior and fully divalent Eu ions (right axis).

$BaAl_4$-type structures [17]. Single crystal x-ray refinements confirm the $I4/mmm$ space group in all compounds reported herein and indicate full occupancy of all lattice sites. In $EuGa_4$ and $EuAl_4$, the Ga and Al atoms occupy two inequivalent crystallographic sites corresponding to the $4d$ site, $M(1)$, at $(0, \frac{1}{2}, \frac{1}{4})$ and the $4e$ site, $M(2)$, at $(0, 0, z)$. Upon substituting Ga for Al, a clear site preference is shown: Al fully occupies the $4d$ site before occupying the $4e$ site. Diffraction data for single crystal x-ray refinements can be found in the Appendix in Table I.

B. Physical properties

Eu $M_{5,4}$-edge x-ray spectromicroscopy was used to probe electronic structure and bonding in selected samples of $Eu(Ga_{1-x}Al_x)_4$ with $x = 0$, 0.18, 0.50, and 1. In general, each of the Eu M_5 and M_4 edges exhibits characteristic multiplet splitting patterns with fine structure that closely resembles expectations from earlier Eu $M_{5,4}$-edge studies of divalent Eu compounds [18,19]. Preliminary calculations in the atomic limit for Eu^{2+} that described transitions from $3d^{10}4f^7$ to $3d^{10}4f^8$ states also reproduced the salient features of the experimental spectra, including the high-energy shoulders observed at approximately 1132.5 eV, as shown in the Appendix in Fig 8. Hence, the Eu $M_{5,4}$-edge spectra support a ground-state Eu^{2+} valence formulation for each $Eu(Ga_{1-x}Al_x)_4$ compound, and no evidence for mixed valence character was detected.

Previous reports showed AFM order in $EuGa_4$ and $EuAl_4$ at $T_N = 15$ and 15.4 K, respectively, and the appearance of spin reorientation transitions in $EuAl_4$ [6,8]. However, in the doped series $Eu(Ga_{1-x}Al_x)_4$ it appears that, as Al replaces Ga(1) at the $4d$ site, multiple spin reorientation transitions occur, while T_N changes nonmonotonously with x. Magnetic susceptibility measurements with $H \| ab$ and $H \| c$ are shown in Figs. 2(a) and 2(b). As many as three magnetic transitions occur down to 1.8 K in $x = 0.50$ and $x = 1$. The magnetic transition temperatures were determined from the temperature derivative of magnetization $d(MT)/dT$ and $C_p(T)$ data [20]. Even though the end compounds order at virtually identical T_N values, it appears that the ordering temperature is significantly enhanced at intermediate compositions and is maximum at $T_N = 19.0$ K near the ordered structure at $x = 0.50$ (purple, Fig. 2). A summary of the magnetic transition temperatures for these compounds is given in the Appendix in Table II.

High-temperature inverse magnetic susceptibility $H/(M - M_0)$ indicates Curie-Weiss behavior across the series as $H/(M - M_0)$ are linear [Fig. 2(c)] above ~25 K. The temperature-independent contribution to the magnetic susceptibility M_0 was subtracted in the case of $EuGa_4$. The linear fits are used to determine the effective magnetic moment p_{eff} and Weiss temperatures θ_W, and these are listed in Table II in the Appendix. The p_{eff} values are comparable to the theoretical $p_{\text{eff}}^{\text{theory}} = 7.94$ for Eu^{2+}, while the θ_W values are positive and close to the T_N temperatures for the whole series. Positive θ_W values are indicative of FM correlations, which were also observed in the isostructural compound $EuRh_2Si_2$ [21].

No crystal electric field (CEF) effects are expected for Eu^{2+} ions, and this is indeed consistent with identical $H \| ab$ and $H \| c$ high-temperature curves, with the $x = 0.50$ data shown in Fig. 2(c) as an example. However, in the ordered state, slight differences in $(M - M_0)/H$ are observed due to the moment orientation relative to the applied field below 50 K, as shown in Figs. 2(a) and 2(b). This is even better evidenced by the anisotropic $M(H)$ isotherms measured at $T = 1.8$ K [Figs. 3(a) and 3(b)]. The magnetization saturation for all measured compounds, except $x = 0$, is $7\mu_B/Eu^{2+}$, as expected for the $J = 7/2$ Hund's rule ground-state multiplet.

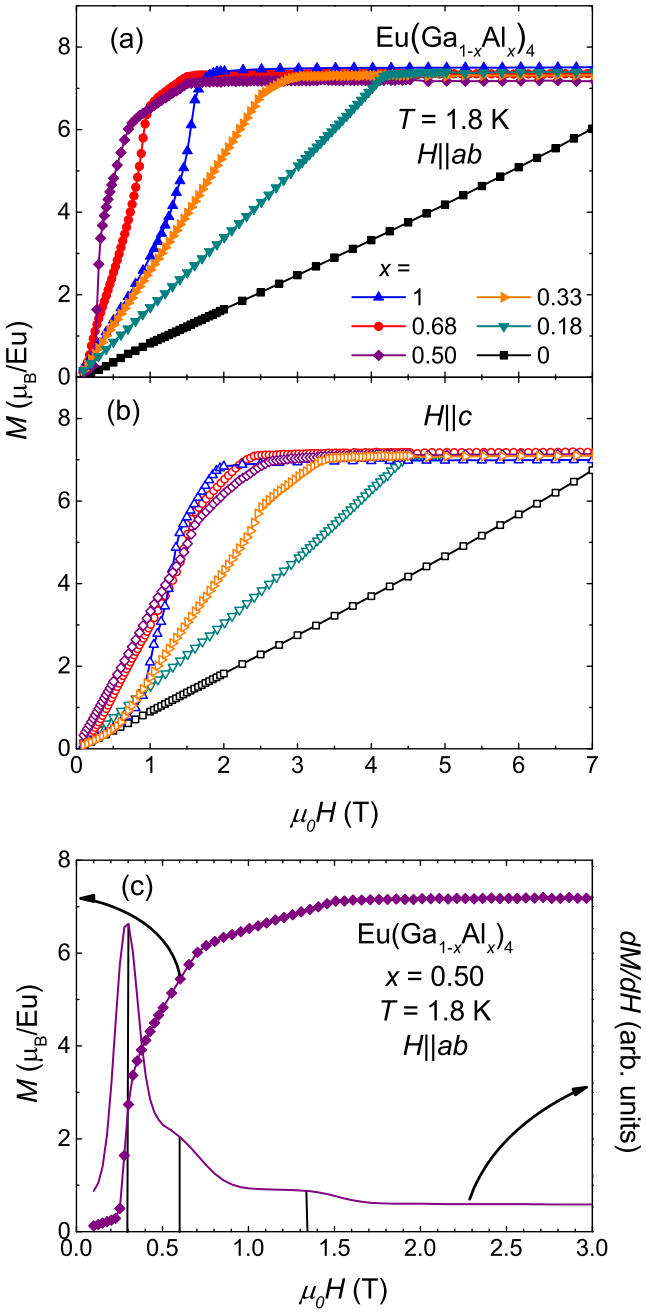

FIG. 3. Field-dependent magnetization curves for (a) $H \| ab$ and (b) $H \| c$ show multiple metamagnetic transitions that are anisotropic. An example of a metamagnetic transition in this series is shown in (c) with an example of how critical fields were determined using peaks from dM/dH vs H.

$EuGa_4$ [black squares, Figs. 3(a) and 3(b)] appears to approach saturation slightly above the 7 T maximum field for these measurements. As Al replaces Ga across the $Eu(Ga_{1-x}Al_x)_4$ series, metamagnetic (MM) transitions are observed for $x =$ 0.33, 0.50, 0.68, and 1 with crystallographic anisotropy. Figure 3(c) shows an example of how the MM critical fields were determined from the peaks in dM/dH. As expected, the number of MM transitions at low T (Fig. 3, $T = 1.8$ K)

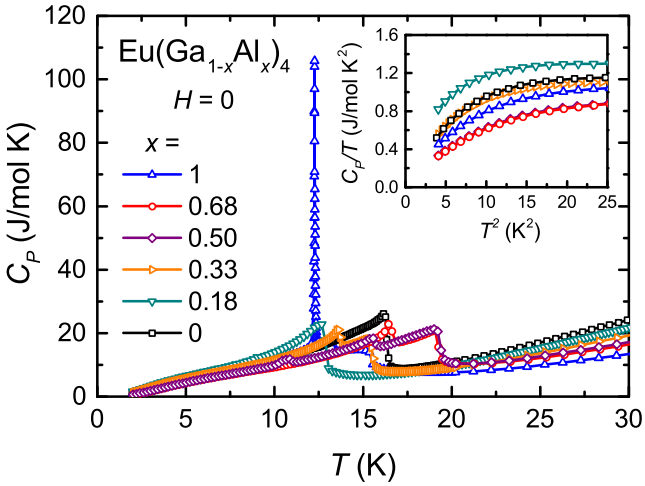

FIG. 4. Specific heat measurements confirm multiple magnetic transitions and a first-order phase transition in $EuAl_4$. The inset shows no evidence of mass renormalization in this system from C_P/T vs T^2.

coincides with the number of transitions in the low H magnetic susceptibility (Fig. 2).

Specific heat measurements (Fig. 4) confirmed the presence of multiple magnetic transitions in these compounds, with the transition temperatures consistent with those derived from temperature-dependent magnetization measurements. Nakamura *et al.* argued for heavy fermion behavior in $EuGa_4$ based on a Fermi liquid relation between the measured quadratic resistivity coefficient A and the calculated electronic specific heat coefficient γ with a modest mass renormalization from $\gamma = 138\ \mathrm{mJ/mol\ K^2}$ [8]. However, our low temperature C_P/T data show no evidence for strong mass renormalization in any of the $Eu(Ga_{1-x}Al_x)_4$ compounds ($x = 0$–1), as shown in the inset of Fig. 4.

No Kondo correlations are present in the $H = 0$ electrical resistivity of $Eu(Ga_{1-x}Al_x)_4$ (Fig. 5). For all x values, the

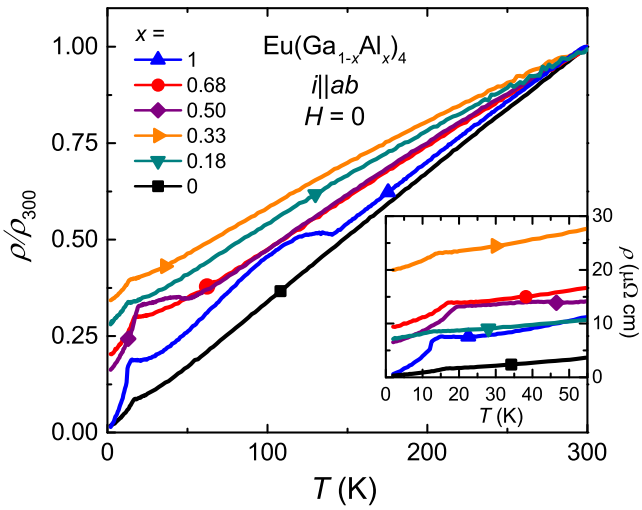

FIG. 5. Temperature-dependent resistivity scaled by ρ_{300}. Anomalies in $x = 0.50$ and 1 are consistent with CDW-like behavior. Inset: Absolute resistivity values at low temperatures.

high temperature resistivity decreases with T, until loss of spin disorder scattering at T_N is marked by an abrupt drop. The residual resistivity ratios (RRR) $= \rho(300\text{K})/\rho_0$ (listed in Table II in the Appendix), with $\rho_0 = \rho(2\text{ K})$, are an order of magnitude larger for the end compounds ($x = 0$ and 1) compared to the doped samples. Remarkably, we observed a sharp resistivity increase occurring for $x = 0.50$ and 1 around 51 and 140 K, respectively. In the latter compound, Nakamura *et al.* [8] associated the resistivity increase at 140 K with a CDW-like transition. Notably, such a transition appears in $Eu(Ga_{1-x}Al_x)_4$ *only* for $x = 0.50$, where (i) x-ray diffraction indicates an ordered structure, with Ga and Al fully occupying the two separate sublattices to form $EuGa_2Al_2$, and (ii) resistivity measurements reveal the lowest residual resistivity ρ_0 and an enhanced RRR value compared to all other doped (disordered) samples.

IV. DISCUSSION AND CONCLUSIONS

Given the chemical similarities between Ga and Al (isoelectronic, similar covalent radii of 1.22 and 1.21 Å, respectively [9]), no substantive differences in crystallographic or physical properties are expected between the isostructural $EuGa_4$ and $EuAl_4$ compounds. However, as Al replaces Ga in $Eu(Ga_{1-x}Al_x)_4$, the magnetic, electronic, and structural properties change nonmonotonously: (i) As shown in Fig. 6(a), a maximum T_N occurs in $x = 0.50$. This is the result of the minimum Eu-Eu ion spacing in this composition, as evidenced by the nonlinear change in the a lattice parameter and unit cell volume [squares and diamonds, respectively, Fig. 6(b)], which are minimum for $x = 0.50$, while c (triangles) increases linearly from $x = 0$ to 1. The ground state across the series is AFM (Fig. 2), even though the spin correlations appear to be FM ($\theta_W > 0, \theta_W \sim T_N$). In the absence of frustration or a CEF effect, magnetic order is likely a result of strong next-nearest-neighbor interactions (with exchange coupling $J_2 > 0$) in addition to the nearest-neighbor Rudermann-Kittel-Kasuya-Yosida coupling (exchange coupling $J_1 < 0$), such that $J_2 > |J_1|$ [22]. This is consistent with the proposed magnetic structure of $EuGa_4$, where intraplane Eu magnetic moments are thought to couple ferromagnetically, while interplane Eu magnetic moments couple antiferromagnetically [21]. (ii) The observation of a possible CDW transition in $Eu(Ga_{1-x}Al_x)_4$ with $x = 0.50$ and 1 may stem directly from the ordered structure, considering the evidence for full site separation for Ga and Al in the $x = 0.50$ compound. This, however, does not explain the lack of a CDW in the $x = 0$ (also ordered) analog, even though applied pressure appeared to induce such a transition [7]. Additional qualitative differences exist even in the pressure dependence of the plausible CDW transition in $EuGa_4$ and $EuAl_4$. According to the change in lattice parameters shown in Fig. 6(b), it seems that Al substituting for Ga acts as positive pressure, resulting in the occurrence of a CDW at $x = 0.50$ in $Eu(Ga_{1-x}Al_x)_4$, similar to the behavior in $EuGa_4$ under applied pressure. (iii) The most notable of the nonmonotonous trends in this series is the minimum in the in-plane lattice parameter a at $x = 0.50$ compared to the linear increase in c across the entire series [Fig. 6(b)]. In order to explain this nonlinear structural trend, density functional theory (DFT) calculations with the local-density approximation were carried out in the linear muffin-tin orbital tight-binding atomic spheres approximation (LMTO-TB-ASA) to probe the bonding character between Al and Ga in the doped compounds.

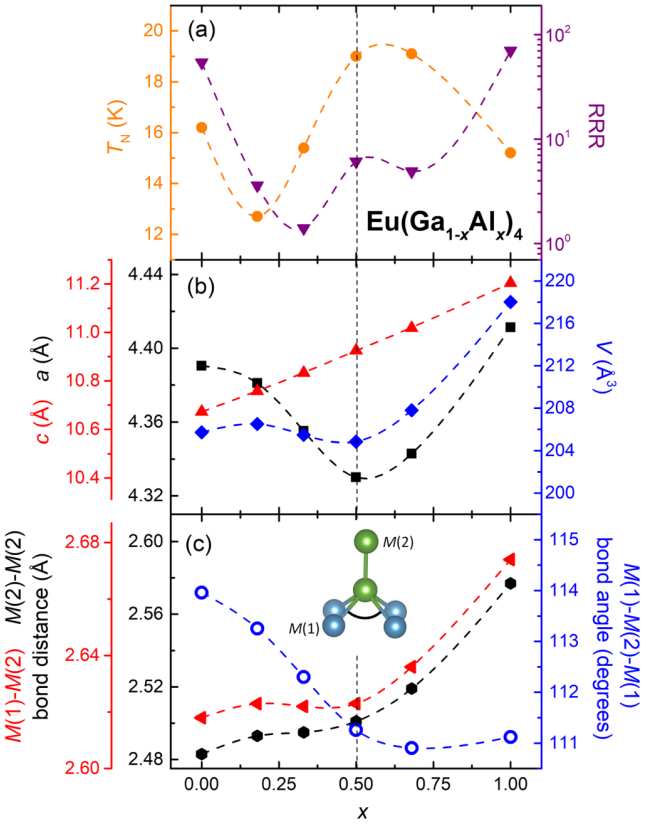

FIG. 6. (a) Increasing x corresponds to a nonmonotonic change in T_N (orange circles) that could be associated with changes in lattice parameters a and c (left axis). RRR values (purple downward triangles) calculated from resistivity measurements show the low amount of disorder in the end compounds and the decreased disorder in $x = 0.50$ compared to other doped compounds in the series (right axis). (b) Lattice parameters a (black squares) and c (red triangles) as a function of doping fraction x, indicating a linear change in c and a nonlinear change in a with increasing x resulting in a local minimum (left axis). Unit cell volume V (blue diamonds) as function of x (right axis). (c) Bond distances between atoms located at the $M(1)$-$M(2)$ (red triangles) and $M(2)$-$M(2)$ (black hexagons) crystallographic sites remain constant up to $x = 0.50$ but increase from $x = 0.50$ to 1 (left axis). The tetrahedral bond angle between $M(1)$-$M(2)$-$M(1)$ atoms (blue open circles) decreases up to $x = 0.50$ and remains constant from $x = 0.50$ to 1 (right axis). All dashed lines are guides to the eye.

DFT calculations were performed for $x = 0, 0.50$, and 1. To avoid complications arising from the unpaired f electrons of Eu^{2+}, Sr^{2+} was substituted as an analog in the calculations. In order to ensure that the nonlinear changes in a were associated solely with the Ga-Al bonds and not the Eu atoms, single crystals of $SrGa_4$, $SrGa_2Al_2$, and $SrAl_4$ were grown from self-flux, and their lattice parameters were measured from powder x-ray diffraction (shown in Fig. 9 in the Appendix). Trends in lattice parameters similar to those in the Eu analogs were observed, with a minimized in $SrGa_2Al_2$ and c increasing linearly from $SrGa_4$ to $SrAl_4$. As expected from the isoelectronic nature of the series, all three band structures are qualitatively very similar

(Fig. 10 in the Appendix). However, analysis of the electron distribution extracted from the integrated density of states (DOS) up to E_F reveals substantive differences between the end compounds and the $x = 0.50$ composition: There is charge transfer from the $M(1)$ to the $M(2)$ site as the composition approaches $x = 0.50$ from both end compounds, such that the $M(1)$ [$M(2)$] electron density is minimum (maximum) for $x = 0.50$ (see the Appendix, Table III). This maximum charge transfer manifests when the two M sites are preferentially occupied by $M(1) =$ Al and $M(2) =$ Ga, implying an enhanced polarization of the $M(1)$-$M(2)$ covalent bond at $x = 0.50$ compared to both $x = 0$ and 1. Despite the similar trends toward less polarization in the Al-rich and Ga-rich compounds, the increased polarization from $x = 0$ to $x = 0.50$ prevents bond length expansion [as $M(1)$ is replaced by Al but $M(2)$ remains occupied by Ga], but then polarization is reduced again from $x = 0.50$ to $x = 1$ [as $M(2)$ is also replaced by Al], resulting in a greater increase in bond lengths.

This unexpected deviation from Vegard's law [23] can be further explained by examining the trends in the $M(1)$-$M(2)$ and $M(2)$-$M(2)$ bond lengths and the $M(1)$-$M(2)$-$M(1)$ bond angle, where $M =$ Al or Ga. As shown in Fig. 6(c), as Al occupies the $M(1)$ site up to $x = 0.50$, the bond distance between $M(1)$ and Ga(2) remains relatively unchanged. However, the bond angle $M(1)$-Ga(2)-$M(1)$ in the Ga-centered tetrahedron decreases linearly up to $x = 0.50$. These crystallographic trends acting together expand the c lattice parameter while simultaneously contracting the a lattice parameter to a minimum. As Al substitutes Ga in the $M(2)$ site up to $x = 1$, a different trend emerges. Here we observe that the tetrahedral bond angle remains constant while the bond lengths between Al(1)-$M(2)$ and $M(2)$-$M(2)$ increase, thus leading to both lattice parameters a and c increasing. These behaviors are likely caused by the greater electronegativity of Ga, which renders the Ga-Ga bonds more polarized.

In summary, we have observed that although Ga and Al are very similar in their valence and size, the substitution of Ga with Al in the doped system $Eu(Ga_{1-x}Al_x)_4$ produces striking and unexpected magnetic, electronic, and structural transitions. The substitution of Ga with Al up to $x = 0.50$ decreases a to a minimum and appears to increase the ferromagnetic interactions in the system, resulting in higher T_N and multiple magnetic transitions. Additionally, temperature-dependent $\rho(T)$ measurements show pronounced changes in electronic transport as manifested by CDW formation in $Eu(Ga_{1-x}Al_x)_4$ for $x = 0.50$ and 1. The CDW behavior is markedly different between $EuAl_4$ and $EuGa_4$, and chemical *and* hydrostatic pressure can be used as tools to elucidate the factors contributing to the CDW formation in this series. Future studies will aim to distinguish between the effects of doping in the magnetic versus the nonmagnetic sublattice in $EuGa_4$ and to explore the effects of hole doping, positive chemical pressure, and disorder on the magnetic and electronic properties of $EuGa_4$.

ACKNOWLEDGMENTS

The authors would like to thank W. Guo, A. Hallas, M. Brando, and F. Steglich for fruitful discussions and N. Botto for performing EMPA measurements. M.S., C.-L.H., and E.M. acknowledge support from the Gordon and Betty Moore Foundation EPiQS initiative through Grant No. GBMF 4417. This paper is funded in part by a QuantEmX grant from ICAM and the Gordon and Betty Moore Foundation through Grant No. GBMF5305 to M.S. The work performed at the University of California, Davis, was supported by Grant No. NSF-DMR-1709382. S.G.M. was supported by the Director, Office of Science, Office of Basic Energy Sciences, Division of Chemical Sciences, Geosciences, and Biosciences Heavy Element Chemistry Program of the U.S. Department of Energy (DOE) at LBNL under Contract No. DE-AC02-05CH11231. Eu $M_{5,4}$-edge spectra described in this paper were measured at the Canadian Light Source, which is supported by the Canada Foundation for Innovation, Natural Sciences and Engineering Research Council of Canada, the University of Saskatchewan, the Government of Saskatchewan, Western Economic Diversification Canada, the National Research Council Canada, and the Canadian Institutes of Health Research. T.M.M. acknowledges support from the Johns Hopkins University Catalyst Award and a David and Lucile Packard Foundation Fellowship for Science and Engineering.

TABLE I. Crystallographic data for single crystals of $Eu(Ga_{1-x}Al_x)_4$ (space group $I4/mmm$). Values for x were determined from EMPA.

Parameter	$x = 0$	$x = 0.18$	$x = 0.33$	$x = 0.50$	$x = 0.68$	$x = 1$
x from free variable refinement	0	0.15	0.31	0.47	0.68	1
a (Å)	4.3904(7)	4.381(3)	4.3551(9)	4.3301(7)	4.3429(13)	4.4113(9)
c (Å)	10.6720(18)	10.757(7)	10.833(2)	10.9253(17)	11.018(3)	11.204(3)
V (Å^3)	205.71(7)	206.5(3)	205.47(9)	204.85(7)	207.80(14)	218.02(11)
Absorption coefficient (mm^{-1})	40.640	36.87	32.93	29.14	23.57	14.968
Measured reflections	1656	969	1734	1725	1769	1722
Independent reflections	137	92	138	139	139	140
R_{int}	0.036	0.031	0.022	0.017	0.047	0.048
Goodness of fit on F^2	1.23	1.20	1.28	1.20	1.12	1.529
$R_1(F)$ for $F^2{}_o > 2\sigma(F^2{}_o)$[a]	0.014	0.024	0.012	0.009	0.015	0.018
$wR_2(F^2{}_o)$[b]	0.037	0.057	0.029	0.021	0.025	0.038
Extinction coefficient	0.0127(11)	0.0022(13)	0.0103(9)	0.0019(5)	0.0019(8)	0.0057(15)
Temperature (K)	90	90	90	90	90	188

[a] $R_1 = \sum || F_o | - | F_c || / \sum | F_o |$.
[b] $wR_2 = \{\sum[w(F_o{}^2 - F_c{}^2)^2] / \sum[w(F_o{}^2)^2]\}^{1/2}$.

TABLE II. Summary of magnetic and transport properties in $Eu(Ga_{1-x}Al_x)_4$.

x	T_N (K)[a] T_2 (K)[a] T_3 (K)[a]	T_N (K)[b] T_2 (K)[b] T_3 (K)[b]	T_N (K)[c] T_2 (K)[c] T_3 (K)[c]	p_{eff}	M_0/H (emu/mol$_{Eu}$)	θ_W (K)	H_{c1} (T) H_{c2} (T) $H\|ab$	H_{c1} (T) H_{c2} (T) $H\|c$	RRR	T^* (K)
0	15.9 13.3	15.9	16.2	8.13	0.0015	6.64	>7 0.6	>7 1	54	
0.18	12.4 8.4	12.4 8.9	12.7	7.91	0	11.16	4.0	4.3	3.6	
0.33	14.9 12.9	14.9 13.4	15.4 13.6	8.15	0	12.26	2.5	3.3 2.4 1.0	1.4	
0.50	17.4 15.4 10.4	18.4 14.9 10.9	19.0 15.6 10.9	7.96	0	22.59	1.5 0.6 0.3	2.4 1.6 1.0	6.1	51
0.68	18.4 15.9	18.4 15.9	19.1 16.4	8.23	0	17.82	1.4 0.9 0.2	2.1 1.5 0.5	4.9	
1	14.9 12.4 10.4	14.4 11.9 10.4	15.2 13.3 12.3	7.98	0	15.02	1.6 1.4	1.8 1.3 1.0	70	141

[a]From $d(MT)/dT$ with $H\|ab$.
[b]From $d(MT)/dT$ with $H\|c$.
[c]From $C_p(T)$.

APPENDIX

Further details of the crystal structures in CIF format for $Eu(Ga_{1-x}Al_x)_4$ with $x = 0$–1 may be obtained from FIZ Karlsruhe [24]. A summary of crystallographic data obtained from single crystal x-ray refinements for $x = 0$–1 is shown in Table I. Thermodynamic data obtained from magnetization and transport measurements can be found in Table II.

To confirm that the anomalous resistivity behavior in $EuAl_4$ is not due to a structural phase transition, powder x-ray diffraction was performed at 300 K and below T^* at 93 K. The diffraction patterns at both temperatures shown in Fig. 7 are consistent with the tetragonal crystal structure of $EuAl_4$, indicating that a phase transition does not occur above 93 K and the charge density wave behavior is not caused by a structural phase transition. The gray bars in this figure indicate the large background peaks contributed by the metal sample holder.

To confirm the fully divalent character of the Eu ions, Eu $M_{5,4}$-edge x-ray spectromicroscopy was used to probe electronic structure and bonding in selected samples of $Eu(Ga_{1-x}Al_x)_4$ for $x = 0, 0.18, 0.50$, and 1. As shown in Fig. 8, the $M_{5,4}$-edge spectra are split by approximately 27.5 eV into low energy M_5 ($3d_{5/2}$) and high energy M_4 ($3d_{3/2}$) edges due to spin-orbit coupling with the $3d$ core hole. The Eu $M_{5,4}$-edge coincides with the onset of the Ga $L_{3,2}$-edge and, for smaller values of x, additional features are apparent and superimposed onto the Eu $M_{5,4}$-edges. The STXM instrument at the spectromicroscopy beamline 10ID-1 at the Canadian Light Source features an elliptically polarizing undulator that deliver photons in the 130 to 2700 eV range [25] to an entrance slitless variable included angle plane-grating monochromator, and the Eu $M_{5,4}$-edge spectral energy resolution was estimated at ± 0.2 eV. Because the density of $Eu(Ga_{1-x}Al_x)_4$ compounds is high, small particle sizes on the order of 0.25 to 1 μm^2 were typically selected using STXM to ensure that the Eu $M_{5,4}$-edge spectra were in the linear regime of the Beer-Lambert law. Multiple spectra from different particles and beam runs were collected and then averaged to improve data quality and signal to background ratio. The Eu $M_{5,4}$-edge data were analyzed in IGOR PRO 7 by first fitting a line to the pre-edge region below 1124 eV, which was subsequently subtracted from the experimental data to eliminate the background of the

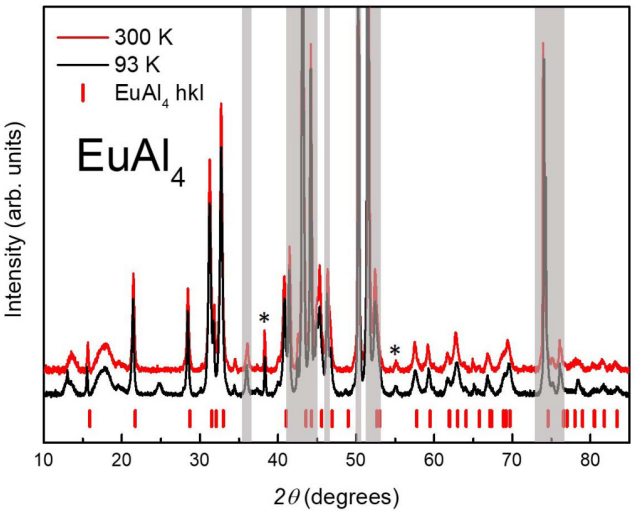

FIG. 7. Powder x-ray diffraction of $EuAl_4$ performed at 300 K (red line) and 93 K (black line). It indicates that the tetragonal space group is preserved above and below the CDW-like transition, and the anomaly in resistivity is not caused by a structural phase transition. Gray bars indicate large background peaks from the metal sample holder, and stars indicate the presence of small amounts of Al flux.

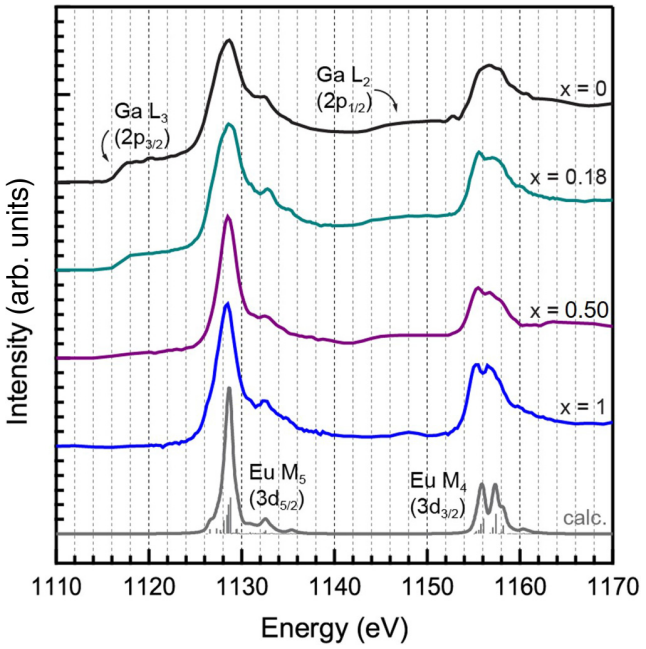

FIG. 8. Experimental Eu $M_{5,4}$-edge spectra of $Eu(Ga_{1-x}Al_x)_4$ and configuration interaction calculation in the atomic limit for Eu^{2+}. Ga $L_{3,2}$-edge features emerge with decreased values of x.

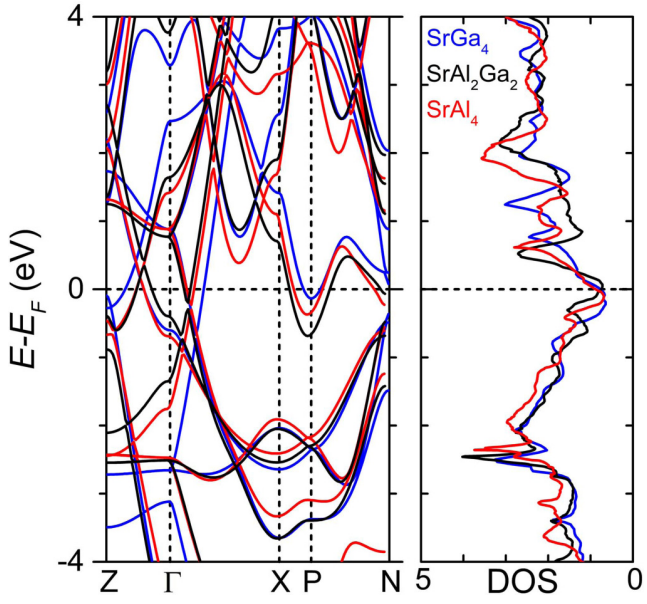

FIG. 10. Band structure calculations for $SrGa_4$, $SrAl_2Ga_2$, and $SrAl_4$. Sr^{2+} is used as a substitute for Eu^{2+} to avoid complications arising from unpaired $4f$ electrons.

spectrum. The data were then normalized by fitting a line to the post-edge region of the spectrum above 1164 eV and setting the edge jump to an intensity of 1.0. Multiplet calculations were implemented as described previously [15,26,27] using CTM4XAS, which is a program based on the original code by Cowan [28] and further developed by de Groot [29,30].

To determine the underlying cause of the nonlinear change in bond lengths as Al is substituted for Ga in $Eu(Ga_{1-x}Al_x)_4$, DFT calculations with the LDA were carried out in the LMTO-TB-ASA implementation for $x = 0, 0.50$, and 1. To avoid complications arising from the unpaired f electrons of Eu^{2+}, Sr^{2+} was substituted as an analog in the calculations. To confirm the validity of this substitution, single crystals of $SrGa_4$, $SrAl_2Ga_2$, and $SrAl_4$ were grown using a self-flux technique as described previously, and the identity of each crystal was confirmed with powder x-ray diffraction. Figure 9 indicates that the Sr analogs of the $Eu(Ga_{1-x}Al_x)_4$ series showed a comparable nonlinear trend in the a lattice parameter, thus justifying their use as analog compounds in these calculations. As expected given the isoelectronic nature of the series, all three band structures are qualitatively very similar, as shown in Fig. 10. All bands have significant bandwidth with two non-symmetry-protected Dirac crossings near the Fermi level. Nonetheless, analysis of the electron distribution extracted from the integrated DOS up to E_F provides insight into the polarization between the $M(1)$-$M(2)$ and $M(2)$-$M(2)$ bonds as illustrated in Table III.

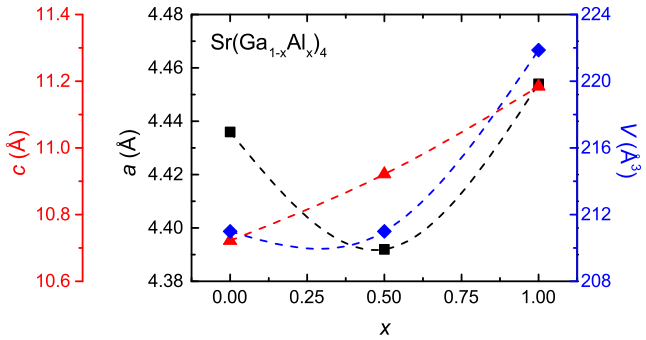

FIG. 9. Lattice parameters from powder x-ray diffraction of $SrGa_4$, $SrAl_2Ga_2$, and $SrAl_4$ single crystals. Trends seen here are consistent with trends observed in the Eu analogs, indicating that the nonlinear change in a is associated with the Ga-Al sublattice.

TABLE III. Analysis of the electron distribution extracted from the integrated density of states up to E_F provides insight into the polarization of the Ga-Al bonds. In contrast to both end members, in $SrAl_2Ga_2$ there is increased charge transfer to the $M(2)$ site. This charge transfer manifests only when $M(1)$ = Al and $M(2)$ = Ga, implying an enhanced polarization in the $M(1) - M(2)$ covalent bonds in $SrAl_2Ga_2$.

Compound	$e^-/M(1)$	$e^-/M(2)$
$SrGa_4$	5.70	4.40
$SrAl_4$	5.63	4.40
$SrAl_2Ga_2$	5.50	4.70
$SrGa_4$ (with $SrAl_2Ga_2$ structure parameters)	5.56	4.40
$SrAl_4$ (with $SrAl_2Ga_2$ structure parameters)	5.75	4.30

[1] M. B. Maple, J. Phys. Soc. Jpn. **74**, 222 (2005).

[2] M. Nicklas, M. E. Macovei, J. Ferstl, C. Krellner, C. Geibel, and F. Steglich, Phys. Status Solidi B **247**, 727 (2010).

[3] T. Takabatake, F. Iga, T. Yoshino, Y. Echizen, K. Katoh, K. Kobayashi, M. Higa, N. Shimizu, Y. Bando, G. Nakamoto, H. Fujii, K. Izawa, T. Suzuki, T. Fujita, M. Sera, M. Hiroi, K. Maezawa, S. Mock, H. v. Löhneysen, A. Brückl, K. Neumaier, and K. Andres, J. Magn. Magn. Mater. **177–181**, 277 (1998).

[4] T. N. Voloshok, N. V. Mushnikov, N. Tristan, R. Klingeler, B. Büchner, and A. N. Vasiliev, Phys. Rev. B **76**, 172408 (2007).

[5] Y. Ōnuki, A. Nakamura, F. Honda, D. Aoki, T. Tekeuchi, M. Nakashima, Y. Amako, H. Harima, K. Matsubayashi, Y. Uwatoko, S. Kayama, T. Kagayama, K. Shimizu, S. Esakki Muthu, D. Braithwaite, B. Salce, H. Shiba, T. Yara, Y. Ashitomi, H. Akamine, K. Tomori, M. Hedo, and T. Nakama, Philos. Mag. **97**, 3399 (2017).

[6] S. Bobev, E. D. Bauer, J. D. Thompson, and J. L. Sarrao, J. Magn. Magn. Mater. **277**, 236 (2004).

[7] A. Nakamura, Y. Hiranaka, M. Hedo, T. Nakama, Y. Miura, H. Tsutsumi, A. Mori, K. Ishida, K. Mitamura, Y. Hirose, K. Sugiyama, F. Honda, R. Settai, T. Takeuchi, M. Hagiwara, T. D. Matsuda, E. Yamamoto, Y. Haga, K. Matsubayashi, Y. Uwatoko, H. Harima, and Y. Ōnuki, J. Phys. Soc. Jpn. **82**, 104703 (2013).

[8] A. Nakamura, T. Uejo, F. Honda, T. Takeuchi, H. Harima, E. Yamamoto, Y. Haga, K. Matsubayashi, Y. Uwatoko, M. Hedo, T. Nakama, and Y. Ōnuki, J. Phys. Soc. Jpn. **84**, 124711 (2015).

[9] B. Cordero, V. Gómez, A. E. Platero-Prats, M. Revés, J. Echeverría, E. Cremades, F. Barragán, and S. Alvarez, Dalton Trans. (21), 2832 (2008).

[10] G. D. Loula, R. D. dos Reis, D. Haskel, F. Garcia, N. M. Souza-Neto, and F. C. G. Gandra, Phys. Rev. B **85**, 245128 (2012).

[11] A. K. Iyer, L. Balisetty, S. Sarkar, and S. C. Peter, J. Alloys Compd. **582**, 305 (2014).

[12] P. H. Tobash and S. Bobev, J. Alloys Compd. **418**, 58 (2006).

[13] M. Stavinoha, J. A. Cooley, S. M. Kauzlarich, C.-L. Huang, and E. Morosan (unpublished).

[14] J. Rodríguez-Carvajal, Phys. B (Amsterdam, Neth.) **192**, 55 (1993).

[15] S. G. Minasian, E. R. Batista, C. H. Booth, D. L. Clark, J. M. Keith, S. A. Kozimor, W. W. Lukens, R. L. Martin, D. K. Shuh, S. C. E. Stieber, T. Tylisczcak, and X.-d. Wen, J. Am. Chem. Soc. **139**, 18052 (2017).

[16] A. B. Altman, C. D. Pemmaraju, S. Alayoglu, J. Arnold, E. D. Bauer, C. H. Booth, Z. Fisk, J. I. Pacold, D. Prendergast, D. K. Shuh, T. Tyliszczak, J. Wang, and S. G. Minasian, Phys. Rev. B **97**, 045110 (2018).

[17] G. J. Miller, F. Li, and H. F. Franzenh, J. Am. Chem. Soc. **115**, 3739 (1993).

[18] G. Kaindl, G. Kalkowski, W. D. Brewer, B. Perscheid, and F. Holtzberg, J. Appl. Phys. **55**, 1910 (1984).

[19] B. T. Thole, G. van der Laan, J. C. Fuggle, G. A. Sawatzky, R. C. Karnatak, and J.-M. Esteva, Phys. Rev. B **32**, 5107 (1985).

[20] M. E. Fisher, Philos. Mag. **7**, 1731 (1962).

[21] Z. Hossain, O. Trovarelli, C. Geibel, and F. Steglich, J. Alloys Compd. **323–324**, 396 (2001).

[22] N. Kumar, S. K. Dhar, A. Thamizhavel, P. Bonville, and P. Manfrinetti, Phys. Rev. B **81**, 144414 (2010).

[23] A. R. Denton and N. W. Ashcroft, Phys. Rev. A **43**, 3161 (1991).

[24] FIZ Karlsruhe, 76344 Eggenstein-Leopoldshafen, Germany [fax: (+49)7247-808-666; email: crysdata@fiz-karlsruhe.de], on quoting the deposition numbers CSD-434440, -434441, -434442, -434443, -434444, and -434445.

[25] K. V. Kaznatcheev, Ch. Karunakaran, U. D. Lanke, S. G. Urquhart, M. Obst, and A. P. Hitchcock, Nucl. Instr. Meth. Phys. Res. **582**, 96 (2007).

[26] M. W. Löble, J. M. Keith, A. B. Altman, S. C. E. Stieber, E. R. Batista, K. S. Boland, S. D. Conradson, D. L. Clark, J. Lezama Pacheco, S. A. Kozimor, R. L. Martin, S. G. Minasian, A. C. Olson, B. L. Scott, D. K. Shuh, T. Tyliszczak, M. P. Wilkerson, and R. A. Zehnder, J. Am. Chem. Soc. **137**, 2506 (2015).

[27] T. A. Pham, A. B. Altman, S. C. E. Stieber, C. H. Booth, S. A. Kozimor, W. W. Lukens, D. T. Olive, T. Tyliszczak, J. Wang, S. G. Minasian, and K. N. Raymond, Inorg. Chem. **55**, 9989 (2016).

[28] R. D. Cowan, *Theory of Atomic Structure and Spectra* (University of California Press, 1981).

[29] F. M. F. de Groot and A. Kotani, *Core Level Spectroscopy of Solids* (Taylor and Francis, New York, 2008).

[30] E. Stavitski and F. M. F. de Groot, Micron **41**, 687 (2010).